PNAS RESEARCH ARTICLE | EARTH, ATMOSPHERIC, AND PLANETARY SCIENCES
ENVIRONMENTAL SCIENCES

Global impacts of an extreme solar particle event under different geomagnetic field strengths

Pavle Arsenović[a,b,1], Eugene Rozanov[c,d], Ilya Usoskin[e], Chris Turney[f], Timofei Sukhodolov[c], Ken McCracken[f], Marina Friedel[b,2], Julien Anet[g], Stana Simić[a], Ville Maliniemi[h], Tatiana Egorova[c], Monika Korte[i], Harald Rieder[a], Alan Cooper[j,1], and Thomas Peter[b]

Affiliations are included on p. 10.

Edited by Guy P. Brasseur, Max-Planck-Institut fur Meteorologie, Hamburg, Germany; received December 15, 2023; accepted May 10, 2024 by Editorial Board Member Akkihebbal R. Ravishankara

Solar particle events (SPEs) are short-lived bursts of high-energy particles from the solar atmosphere and are widely recognized as posing significant economic risks to modern society. Most SPEs are relatively weak and have minor impacts on the Earth's environment, but historic records contain much stronger SPEs which have the potential to alter atmospheric chemistry, impacting climate and biological life. The impacts of such strong SPEs would be far more severe when the Earth's protective geomagnetic field is weak, such as during past geomagnetic excursions or reversals. Here, we model the impacts of an extreme SPE under different geomagnetic field strengths, focusing on changes in atmospheric chemistry and surface radiation using the atmosphere–ocean–chemistry–climate model SOCOL3-MPIOM and the radiation transfer model LibRadtran. Under current geomagnetic conditions, an extreme SPE would increase NO_x concentrations in the polar stratosphere and mesosphere, causing reductions in extratropical stratospheric ozone lasting for about a year. In contrast, with no geomagnetic field, there would be a substantial increase in NO_x throughout the entire atmosphere, resulting in severe stratospheric ozone depletion for several years. The resulting ground-level ultraviolet (UV) radiation would remain elevated for up to 6 y, leading to increases in UV index up to 20 to 25% and solar-induced DNA damage rates by 40 to 50%. The potential evolutionary impacts of past extreme SPEs remain an important question, while the risks they pose to human health in modern conditions continue to be underestimated.

solar particle event | geomagnetic field | geomagnetic excursion | ozone | radiation dose

Significance

The ozone layer protects life on Earth by absorbing solar ultraviolet (UV) radiation ~15 to ~35 km above the surface. The ozone layer can be depleted by solar particle events, which are short-lived bursts of high-energy particles which can alter atmospheric chemistry. Currently, the Earth's geomagnetic field deflects these particles, limiting their impact to the polar regions. However, geological records demonstrate periods throughout Earth's history where the geomagnetic field significantly weakened. During those periods, cosmic ionizing particles can enter Earth's atmosphere at lower latitudes and damage the ozone layer, resulting in marked increases in surface UV radiation. Potential consequences include serious health hazards and longer-term climatic and evolutionary impacts.

The Earth's magnetic field plays a critical role in protecting life by shielding it from ionizing solar and galactic cosmic rays. Solar particle events (SPEs) are phenomena when charged particles, mostly protons, are accelerated in the solar corona and interplanetary space to high (sometimes near-relativistic) energies, producing powerful bursts of ionizing particles (1) that can penetrate the Earth's atmosphere. The current strength of the geomagnetic field deflects most cosmic high-energy particles away from the Earth and limits penetration to the lower levels of the atmosphere mostly to the polar regions, where the geomagnetic field lines are vertically oriented (2). While the duration of these sporadic solar events is short (on the order of hours to days), the resulting levels of ionizing radiation can be very large and have diverse environmental and technological impacts, including damage to the ozone layer, spacecraft and astronauts, and disruptions to telecommunications systems (3). Hundreds of weak SPEs occur during a typical 11-y solar cycle (1, 4), with a higher probability during the maximum and descending solar phases, but much stronger SPEs are known to have occurred in the recent past. Furthermore, extreme SPEs, up to three orders of magnitude stronger than any observed in the satellite era, have been recently found in paleorecords such as tree rings and ice cores (3, 5, 6), with well-known events in, e.g., years 993 CE, 775 CE, 660 BCE, 5259 BCE, and 7176 BCE. These paleorecords indicate that major SPEs occur roughly every few millennia (7), but the full physical and biological impacts of these events through time remain unclear. In the modern world, they would have a diverse range of serious effects on technological systems (3). As an example, while the well-known 1859 solar storm known as the "Carrington Event" is not known to have been accompanied by a SPE (8), it had widespread impacts on the atmosphere, telegraph communications, and electrical infrastructure.

The ozone layer located in the stratosphere (15 to 50 km above the Earth's surface) serves as a critical shield against solar ultraviolet (UV) radiation, protecting all life forms on the Earth's surface and troposphere (from the surface to about 15 km altitude). The high-energy particles associated with a SPE can deplete ozone in both the stratosphere,

The authors declare no competing interest.

This article is a PNAS Direct Submission. G.P.B. is a guest editor invited by the Editorial Board.

[1]To whom correspondence may be addressed. Email: science@pavle.de or alacooper@csu.edu.au.

[2]Present address: Leipzig Institute for Meteorology, University of Leipzig, Leipzig 04103, Germany.

This article contains supporting information online at https://www.pnas.org/lookup/suppl/doi:10.1073/pnas.2321770121/-/DCSupplemental.

Published July 1, 2024.

as well as the higher atmospheric layer, the mesosphere (50 to 80 km above ground) (9). The ozone reduction occurs when the high-energy particles ionize air molecules, creating reactive species such as nitrogen oxides NO_x (N, NO, and NO_2) (10, 11) and hydroxyl radicals HO_x (H, OH, and HO_2) (12, 13) both of which destroy ozone through catalytic cycles. The resulting large-scale changes in the middle atmosphere alter fundamental atmospheric properties, such as the equator-to-pole temperature gradient (2), impacting conditions all the way down to the surface. Overall, however, the short duration of SPEs means that they currently have little impact on ozone climatology. Elevated NO_x levels typically decay a few weeks after a SPE (14–16) and are only associated with ozone destruction for about a month (17–19). In extreme cases, ozone anomalies and surface temperature changes have been modeled to last from half a year (20) to a few years (21) in the modern era.

Geological records show many periods when Earth's geomagnetic field strength was greatly reduced compared to the relatively strong field of modern times. These periods include events such as geomagnetic polarity reversals (when the magnetic poles switch) and geomagnetic field excursions (a pronounced reduction of geomagnetic field strength, but without long-term polarity inversion), and can be observed back as far as the Ediacaran period (22, 23). During such phases of greatly reduced geomagnetic field strength, the biophysical consequences of SPEs could be very large, as solar particles would precipitate over a much larger proportion of the Earth's surface, including lower latitudes. While geomagnetic reversals are relatively rare in the geological record, typically occurring every 0.1 to 1 Ma (24, 25), excursions are far more common, although their properties are less well known (26). Recent geological records suggest that excursions may occur on timescales of <10 ka, with each event characterized by a significant reduction in the geomagnetic dipole component for hundreds to thousands of years (27). The prolonged periods of weak geomagnetic strength that characterize excursions or reversals (27) (on the order of several millennia) raise the possibility that one or more extreme SPEs are likely to occur during the same period. Under such circumstances, the cosmic radiation shielding normally provided by the geomagnetic field would collapse, leaving only that provided by the atmosphere, with likely serious impacts on atmospheric and biological systems. Interest in these events has increased considerably since satellite and other observations suggest that the Earth's geomagnetic field has weakened by ~10% over the last century (28), prompting speculation about whether this trend might indicate an upcoming excursion or even a full reversal (24–26, 29–33).

Grand solar minima (GSM), periods of markedly decreased solar activity where sunspots almost or completely disappear for multiple decades, are further important solar phenomena which impact the levels of cosmic radiation reaching Earth. The decreased strength of the solar wind during GSM allows higher fluxes of strongly ionizing galactic radiation to impact Earth's atmosphere, due to the reduced protection from the interplanetary solar magnetic field created by the solar wind (2). Over the past 10,000 y, GSM appear to have occurred about 1 to 2 times per millennium and lasted 30 to 150 y (34). The extended duration of lowered solar activity in a GSM means the effects on Earth are much more clearly visible in the climate records (35) than those of SPEs. Conversely, while the effects of SPEs are much shorter in time, the impacts can be much stronger. The effects of GSM on atmospheric chemistry and climate have recently been modeled for the most recent major geomagnetic excursion, the Laschamps Event 42,000 B.P., where 6 to 7 GSM can be observed in dendrorecords (36). However, the specific impact of a large SPE on the Earth's atmosphere during a period of weak geomagnetic field strength remains unclear, including the repercussions on terrestrial life and human health. Previous studies have either used simplified atmospheric models (37–39) or did not consider geomagnetic field variations (20, 40, 41).

To address this issue, we model the impact of an extreme SPE comparable in size to the largest events detected over the past few millennia (3, 5, 6), which is about a hundred times stronger than the most powerful directly observed in recent history, specifically the event of February 23, 1956 (42). We also model the extreme SPE during a geomagnetic excursion with a total absence of geomagnetic field. While questions remain about the degree of dipole field strength loss during different geomagnetic excursions (43), this approach allows investigation of the full spectrum of potential atmospheric responses under the most severe conditions.

For this purpose, we use the advanced coupled atmosphere–ocean–chemistry–climate model SOCOL3-MPIOM (44, 45) and the radiative transfer model LibRadtran (46). SOCOL3-MPIOM accounts for the important feedback between atmospheric composition, radiation, and dynamics and is specifically designed to describe the atmospheric effects of energetic particles (47). LibRadtran allows accurate calculations of the propagation of solar radiation in the Earth's atmosphere. The combination of these models is ideally suited to study the effects of extreme energetic particles on atmospheric chemistry and surface UV levels.

Results

The short- and long-term impacts of extreme SPEs on the atmosphere and their modulation by the geomagnetic field strength are presented as mean annual differences and global mean monthly changes between simulations, with and without the SPE. The statistical significance of our results was determined using Student's *t* test at the 99% confidence level.

NO_x Impact. In the mesosphere, while NO_x is generated through the ionization of atmospheric molecules by energetic particles, the resulting concentrations are closely tied to the photolytic-loss process driven by solar wavelengths around 180 and 190 nm (48). Photolysis of NO releases N, which then reacts with a further NO molecule to produce stable N_2 and O, effectively reducing NO_x in the atmosphere (49). While these wavelengths play a pivotal role in mesospheric NO_x chemistry, the pronounced absorption at that altitude means that UV radiation at these wavelengths is greatly reduced in the underlying stratosphere (48). However, in the polar night regions the photolytic reaction ceases, extending the mesospheric NO_x lifetime (to days-months) and allowing it to be propelled down to stratospheric altitudes by the downwelling air motion within the polar vortex. As a result, NO_x can influence stratospheric ozone dynamics in regions distant from the initial production zones.

The simulations (*Material and Methods*) indicate that after an extreme SPE, substantial increases in atmospheric NO_x are observed under either current conditions or during a geomagnetic excursion (Fig. 1 *A* and *B*), followed by decay over several years. The stratospheric NO_x levels remain elevated for up to 3 y under current conditions, but for considerably longer during a geomagnetic excursion. Under present-day conditions, an extreme SPE would generate large amounts of NO_x throughout the whole mesosphere and the polar stratosphere, with the largest stratospheric increases (20 to 80 ppb) observed above the poles (Fig. 2 *A*–*D*). For example, a >200% increase in NO_x over the North Pole due to the downwelling of the mesospheric NO_x during the polar night. Increases are also seen in the tropical mesosphere and

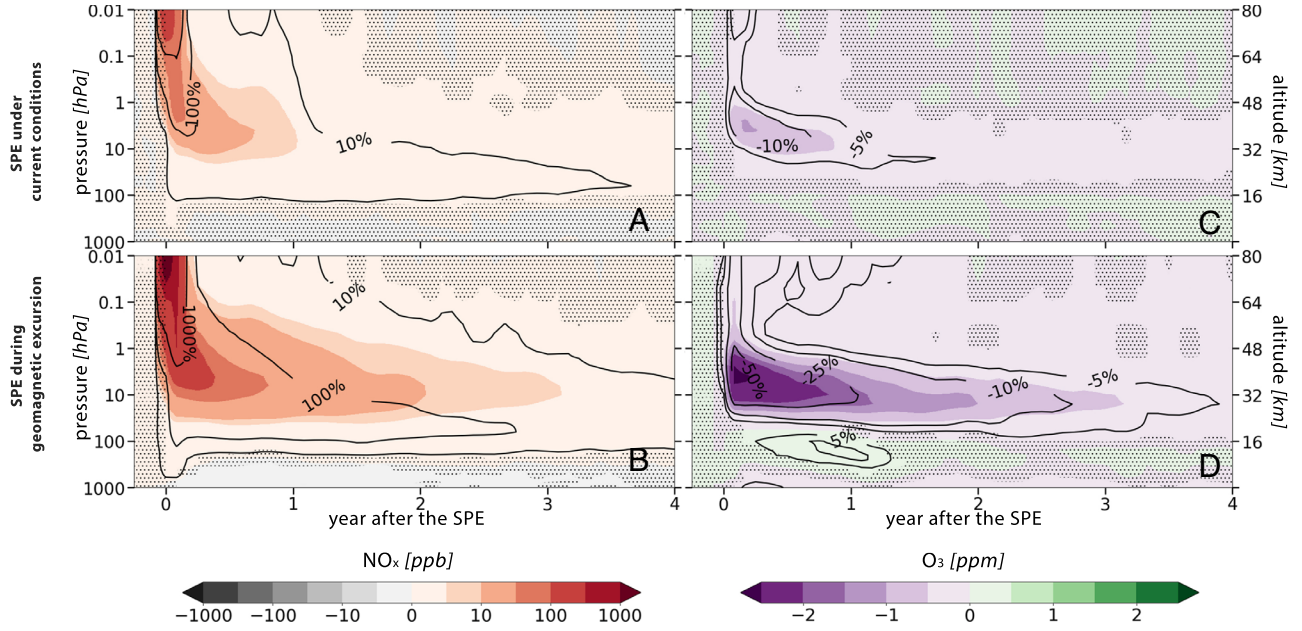

Fig. 1. Global monthly mean NO_x (*A* and *B*) and O_3 (*C* and *D*) response to the SPE under current conditions (*A* and *C*) and during a geomagnetic excursion (*B* and *D*). Color intervals for NO_x: −1,000, −500, −100, −50, −10, −5, 0, 5, 10, 50, 100, 500, and 1,000 ppb; for O_3: steps of 0.5 ppm. The solid contour lines overlaid on the color intervals indicate the percentage differences in NO_x and O_3 levels between simulations with and without SPE, with nonshaded areas highlighting statistical significance at the 99% confidence level (Student's *t* test).

mid-latitude stratosphere as NO_x-rich air from the polar regions mixes with surrounding air following the polar vortex breakup. As expected, these impacts are much more severe during a geomagnetic excursion (Fig. 2 *E*–*H*) with intense and widespread increases in NO_x, exceeding 500% in the northern polar stratosphere. The absence of a geomagnetic field allows solar particles to precipitate uniformly across latitudes, leading to significant NO_x increases (20 to 80 ppb) in the tropical upper atmosphere (mesosphere and stratosphere), while NO_x concentrations double in the upper southern polar troposphere.

HO_x Impact. In contrast to NO_x, HO_x has a short lifetime (seconds-hours) in the stratosphere and mesosphere. Although HO_x destroys ozone in a fast catalytic cycle, it also rapidly engages in self-reaction within the HO_x family, where OH and HO_2 neutralize each other to form water and molecular oxygen. Additionally, OH reacts with NO_2, leading to the formation of nitric acid (HNO_3) (49). Due to this fast reactivity and consequent short lifetime, HO_x does not get transported like NO_x and therefore only plays a vital role in ozone chemistry in regions where it is produced.

During an extreme SPE, a notable surge in HO_x radicals arises within the mesosphere (*SI Appendix*, Fig. S2). However, the short-lived nature of the HO_x radicals makes their presence statistically insignificant in the context of HO_x annual mean enhancements. Within the stratosphere, SPE-enhanced levels of NO_x react with HO_x originating from the troposphere (from water vapor, methane, and molecular hydrogen) to produce nitric acid, thus creating statistically significant decreases in stratospheric HO_x.

Ozone Impact. Fig. 1*C* displays the area-weighted global mean ozone changes caused by a SPE in the current geomagnetic state. In the months after the SPE, marked by substantial increases in NO_x and HO_x species, a notable decrease in upper mesospheric ozone concentrations occurs. However, after the initial depletion, ozone levels return to baseline values within just 4 to 5 mo. Similarly, stratospheric ozone levels remain reduced by around 10% in the upper stratosphere (10 to 1 hPa), mostly due to NO_x, for almost a year after the SPE. In contrast, when the SPE occurs during a geomagnetic excursion a much stronger reduction in global mean ozone ensues (Fig. 1*D*). Mesospheric ozone diminishes by 25% immediately after the event and stays reduced by roughly 10% throughout the entire first year. Stratospheric ozone declines by 50% after the event and is still reduced by around 5% 4 y later.

The model predicts that under current geomagnetic field conditions, ozone levels would decrease in the northern polar upper stratosphere by 30% in the first year (Fig. 3*A*), with a smaller decrease in the southern polar upper stratosphere, and then gradually recover over the next 2 y (Fig. 3 *B*–*D*). As expected, during a geomagnetic excursion the ozone destruction is much more severe. In the first year, ozone is reduced by up to 50% in northern and ~40% in southern high latitudes (Fig. 3*E*), with poleward transport of tropically generated ozone-depleted atmospheric conditions contributing to the high latitude signal. The recovery process also takes longer, with stratospheric levels being still suppressed by 10 to 20% 3 y later (Fig. 3 *F*–*H*).

In terms of the total ozone column (Fig. 4), large decreases are predicted under current geomagnetic conditions for high-latitude regions (~12% in the south, ~8% in the north) but only minor changes in tropical areas. However, during a geomagnetic excursion, the ozone reductions manifest on a global scale (12 to 16%), with particularly severe impacts in the polar regions, which persist to the third year (~12%), after which the signal gradually dissipates. Due to the magnitude of the extreme SPE, these ozone losses are markedly larger than those modeled for the SPEs of August 1972 and October 1989, which were linked to decrease in polar ozone of around 1% (50). It is interesting to note that the modeled first-year polar ozone column loss shows remarkable similarities to the effects of the recent "ozone hole," when the peak depletion in the 1990s is compared with the 1970 to 1980 period via the ozone column reanalysis database MSR2 (51).

Radiation Doses. Given the varying impacts of an extreme SPE on ozone concentrations, we used the LibRadtran model to calculate the changes in incoming solar shortwave radiation at ground-level under clear skies, along with the resulting potential effects on key

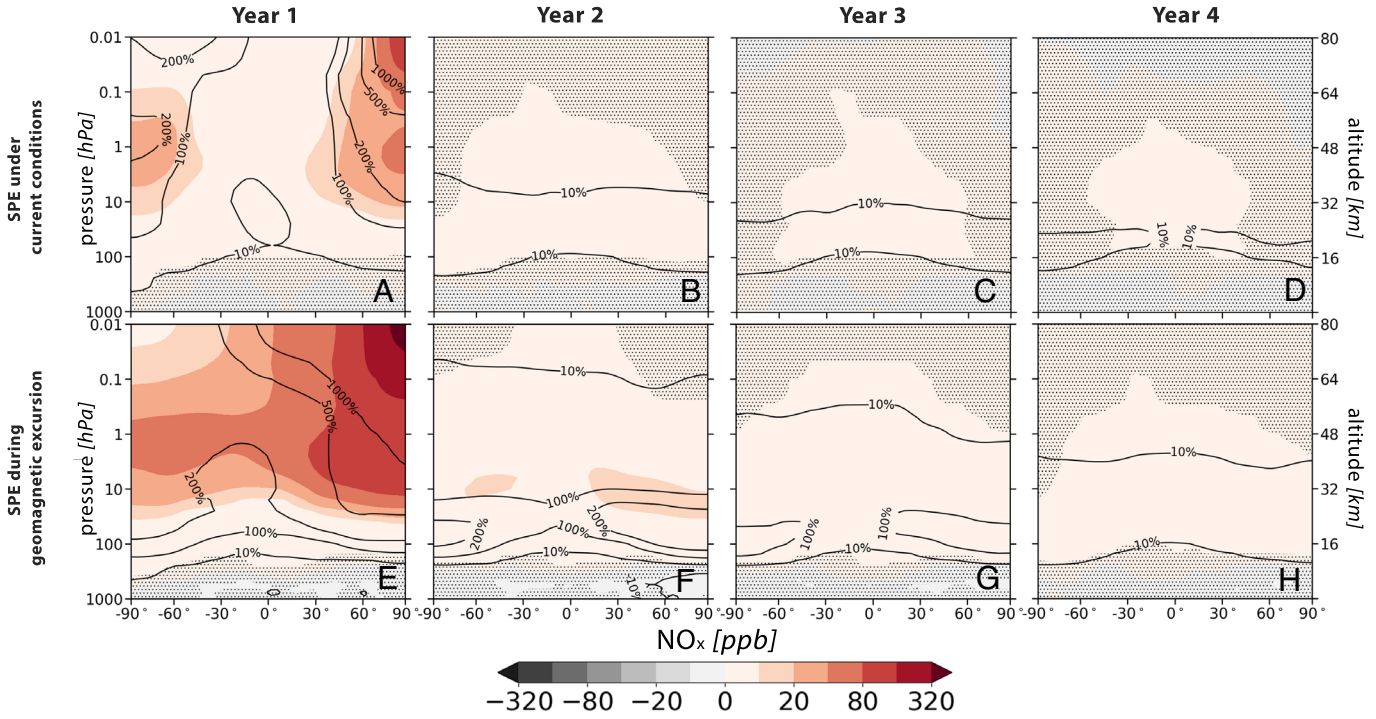

Fig. 2. Annual zonal mean NO_x response to the SPE under current conditions (*A–D*) and during a geomagnetic excursion (*E–H*). Color intervals: −320, −160, −80, −40, −20, −10, 0, 10, 20, 40, 80, 160, and 320 ppb. The solid contour lines overlaid on the color intervals indicate the percentage differences in NO_x levels between simulations with and without SPE, with nonshaded areas highlighting statistical significance at the 99% confidence level (Student's *t* test).

parameters such as UV Index, DNA damage, and synthesis of previtamin D_3 in human skin.

Under current geomagnetic conditions, the model shows the most significant changes in the UV-B (280 to 315 nm) range of the solar spectrum at the Earth's surface, with the largest increases occurring at the shortest wavelengths, which are known to be particularly damaging to DNA, proteins, and biological systems (52). Immediately after the SPE, solar UV radiation increases across most of the spectrum, with the largest relative increases (over 80%) observed around 290 nm over all the continents (Fig. 5). It takes 3 y for UV-B radiation levels to return to their original values.

In contrast, a SPE during a period of deteriorated geomagnetic field results in extreme increases in surface UV radiation across

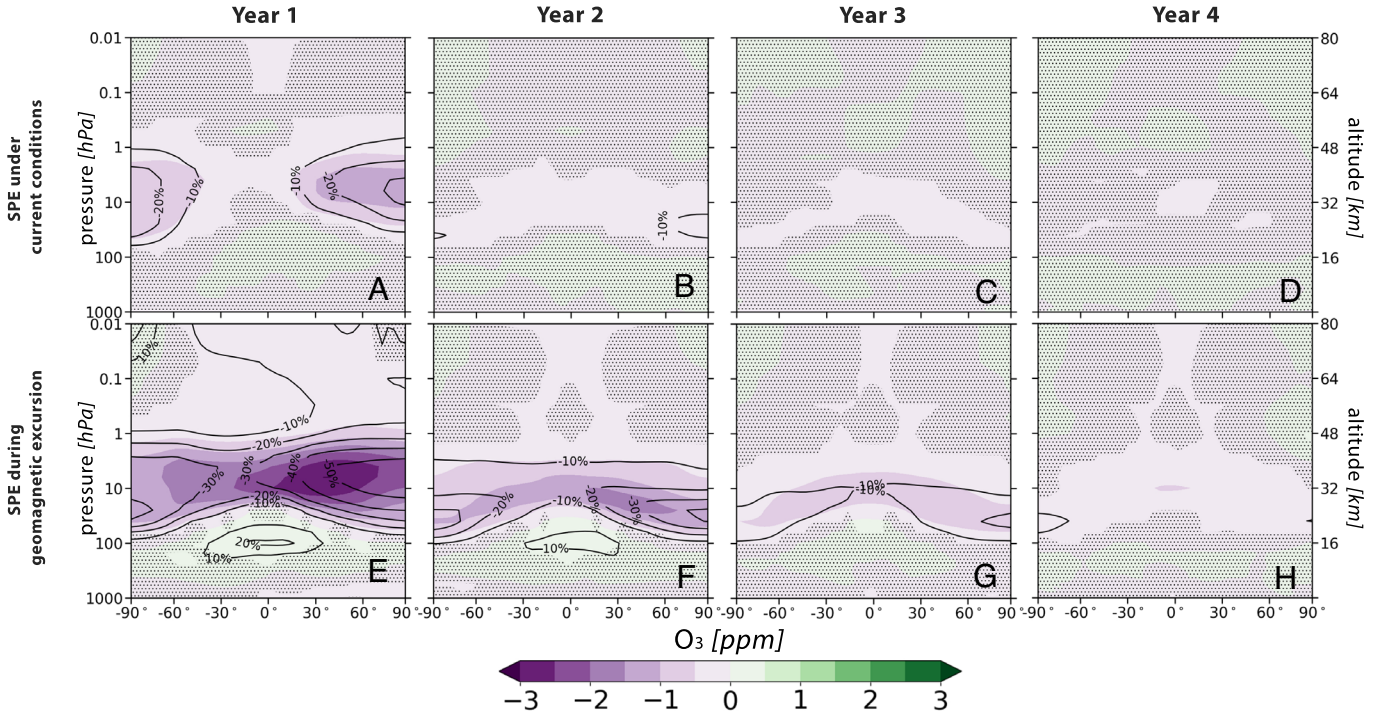

Fig. 3. Annual zonal mean O_3 response to the SPE under current conditions (*A–D*) and during a geomagnetic excursion (*E–H*). Color intervals: steps of 0.5 ppm. The solid contour lines overlaid on the color intervals indicate the percentage differences in O_3 levels between simulations with and without SPE, with nonshaded areas highlighting statistical significance at the 99% confidence level (Student's *t* test).

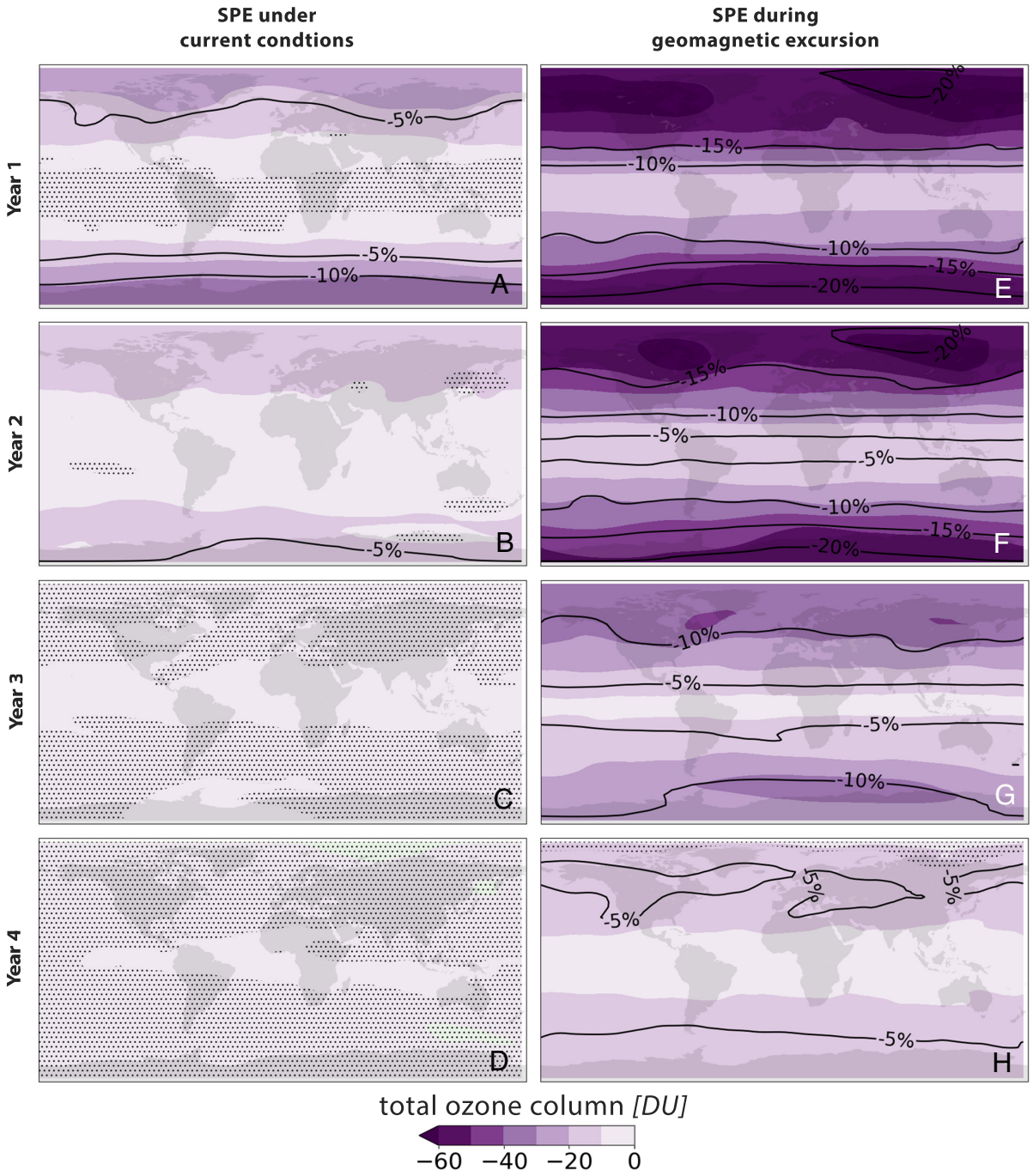

Fig. 4. Annual mean total ozone column response to the SPE under current geomagnetic conditions (*A*–*D*) and during excursion (*E*–*H*). Color intervals: steps of 10 DU. The solid contour lines overlaid on the color intervals indicate the percentage differences in total ozone column between simulations with and without SPE, with nonshaded areas highlighting statistical significance at the 99% confidence level (Student's *t* test).

the UV-B spectrum, including >320% for shorter wavelengths (290 nm), and remains elevated for 5 to 6 y. The increase in the 300 to 310 nm band of up to 30% in the first year (*SI Appendix*, Fig. S3) is crucial as it corresponds to the peak mutagenicity wavelengths for skin carcinogenesis (53). A similar increase of up to 10% is seen at 313 nm, while the somewhat smaller increase in the 310 to 320 nm waveband includes wavelengths that contribute to the total mutagenic effect and reflects a broader skin cancer risk associated with UV exposure (54). These elevated levels, even if relatively short-lived, would have pronounced impacts not just on climate systems but also on biological cycles, especially those based around primary producers utilizing photosynthesis, such as aquatic ecosystems (55). UV-B is known to have pronounced negative impacts on these systems, and aquatic microbiomes more generally (including bacteria, zooplankton, cyanobacteria, and corals), as well as on macroinvertebrates, amphibians, fish, and other groups where damage to larvae, eyes, and DNA are common effects (56). These results highlight the potential risks to biological systems posed by an extreme SPE.

UV Index. From a human perspective, one of the most obvious consequences of elevated UV-B levels is the increased risk of sunburn (erythema) and associated health effects. The clear-sky erythemal irradiance is quantified with the UV Index or UVI, which is a measure of the intensity of UV radiation in terms of causing sunburn in human skin. Our models predict that a SPE

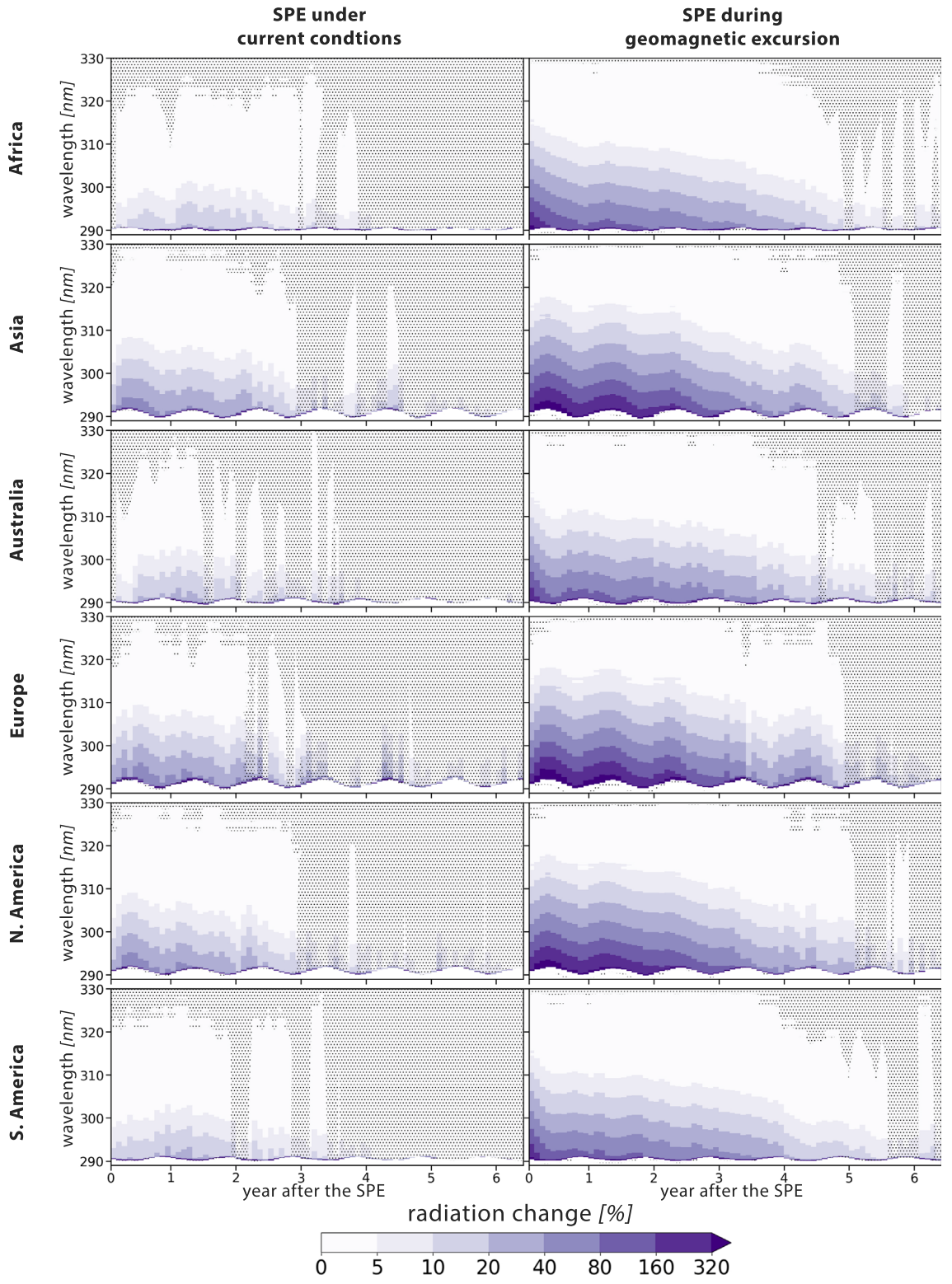

Fig. 5. Response of solar spectral irradiance at the Earth's surface over continents for the first 6 y after the SPE under current conditions (*Left*) and during a geomagnetic excursion (*Right*) shown as a function of wavelength. Nonshaded areas are statistically significant at the 99% confidence level (Student's *t* test).

under modern conditions would result in a significant increase in erythemal radiation across all continents (Fig. 6). The relative increase is ~5% over North America, Europe, and Asia, and 2 to 3% over South America, Africa, and Australia, persisting for 2 to 3 y after the SPE. However, during a geomagnetic excursion there are much more severe global increases in the UV Index, with a 25% increase in the first year over Europe, North America, and Asia. As an example, the time to develop sunburn for Caucasian skin under sunny European conditions (e.g., UVI 8) could be as little as 18 min (57). Over South America, Africa, and Australia, the increase in UVI spikes to around 20% immediately after the event and dissipates slowly over the following months, with levels still elevated by 10% in the second year. The elevated UVI levels take 5 to 6 y to become negligible.

Another serious consequence of elevated UV-B radiation is the immediate damage to the eyes, such as snow blindness, which can

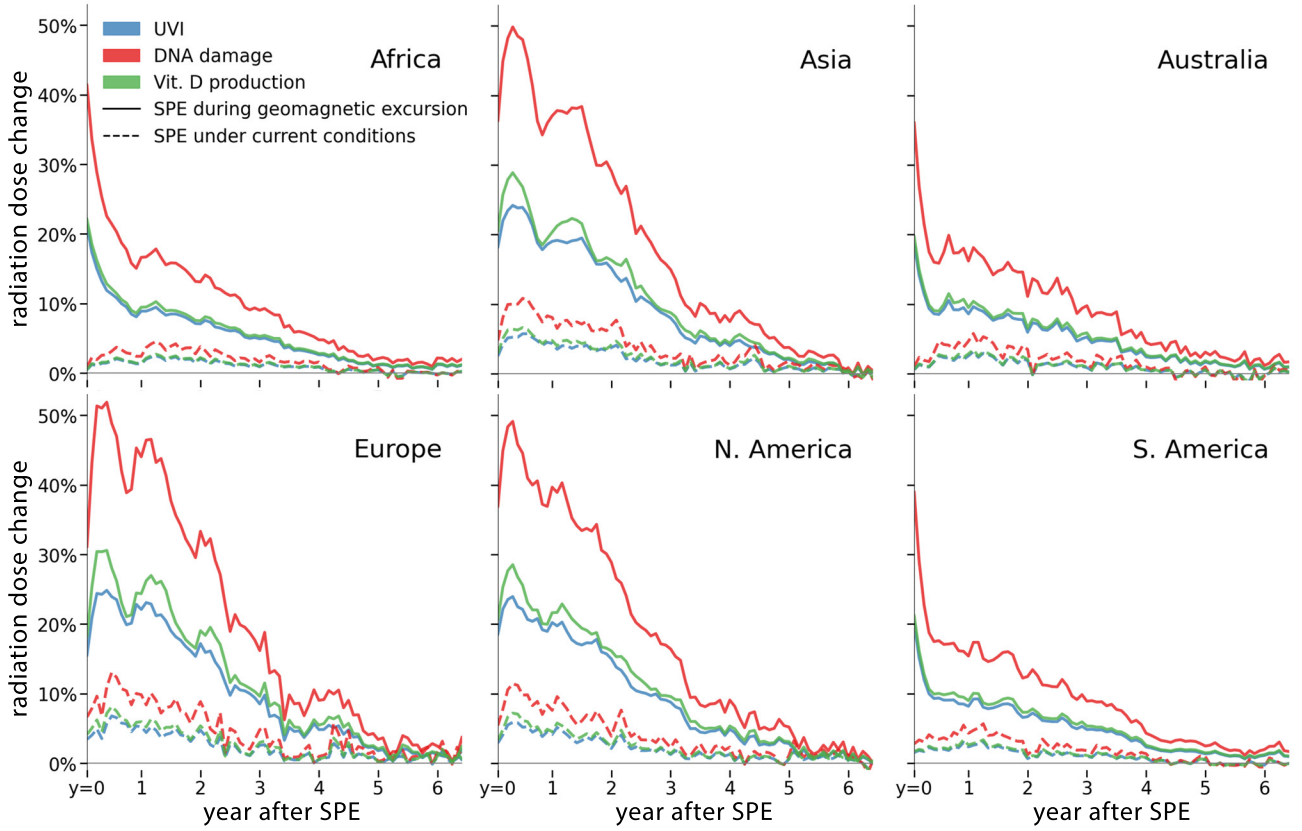

Fig. 6. UVI, vitamin D production, and DNA damage response for different continents over the first 6 y after the SPE (y = 0) under current conditions (dashed line) and during a geomagnetic excursion (solid line).

occur rapidly with exposure, while more prolonged exposure may lead to the development of cataracts over time. Photokeratitis, also known as snow blindness, occurs when the epithelial layer covering the cornea is sunburned and peels off, exposing the corneal nerves. The corneal epithelium absorbs almost 100% of UV radiation below 290 nm, making it particularly vulnerable to changes in UV-B levels. As a result, using the UVI to quantify ocular damage has been shown to considerably underestimate the risk of ocular damage from UV-B exposure [particularly in the ~290 nm wavelength range most impacted by atmospheric ozone decrease; (58)]. This risk can be increased further by reflective surfaces such as snow cover, which can reflect up to 88% of solar UV-B radiation (59). Clearly, photokeratitis could pose a significant risk to human populations when a SPE occurs during weak geomagnetic field conditions.

Vitamin D Production. UV-B radiation initiates the synthesis of vitamin D_3 (cholecalciferol) in the human skin, an essential regulator of calcium levels, and is considered one of the few beneficial health effects of UV radiation (60). Due to the increased UV radiation following a SPE, human vitamin D production rates would be projected to increase (Fig. 6), although this depends on individual characteristics including skin type. It should also be noted that there is little evidence that excessive vitamin D production is possible from sunlight exposure, or that elevated levels of vitamin D would be unhealthy (61). Nevertheless, ancient DNA and genetic selection studies have shown that skin pigmentation genes have been one of the most frequent targets of genetic selection in recent human evolution (62). This has been related to the initial movement from high UV-B sub-Saharan African environments to locations across Eurasia where UV-B levels were much lower (63) and varied regionally and over time. The genetic selection for skin pigmentation is thought to reflect a balance between the need for vitamin D production and other effects and protection from UV-B damage.

We have calculated theoretical vitamin D production by applying the CIE-174 (64) action spectrum to the LibRadtran output (*SI Appendix*, Fig. S3). Under current conditions, we find in the months after the SPE an increase in vitamin D production of 5 to 7% over the northern continents, but only a few percent in the Southern Hemisphere. In contrast, during a geomagnetic excursion, vitamin D production rates are predicted to increase by ~30% over northern and ~20% over southern continents, respectively, in the months after the SPE and track the UVI levels.

DNA Damage. An important consequence of UV radiation is increased rates of DNA damage. This occurs mostly through the formation of pyrimidine dimers, leading to mutations in dividing cells and potentially causing carcinogenesis. The risk and impacts of damage vary according to species and environment (52, 55). The DNA damage caused by increased radiation exhibits similar behavior to UVI, and vitamin D, but with a stronger response (Fig. 6). Under current geomagnetic conditions, a SPE is estimated to increase DNA damage rates by 10% over Europe, North America, and Asia and 5 to 6% over Australia, South America, and Africa. This increase diminishes to near zero by 3 to 4 y after the event.

During a geomagnetic excursion, human DNA damage is predicted to increase by as much as 50% over Europe, North America, and Asia in the first year after the SPE. This drops to 35 to 40% by the end of the first year, followed by another increase in the next summer season of 40 to 45%. Over the southern continents, the initial spike amounts to ~40%, which halves a few months after the SPE, and then declines linearly. However, it takes 6 y

after the event before DNA damage rates become indistinguishable from the reference simulation across all continents.

Discussion

An Extreme SPE under Current Conditions. Current concerns about SPE events focus on the extent of technologies in the modern interconnected world that are deeply exposed to space weather events and the inability to predict the timing of the next extreme SPE (65). For example, satellites are particularly vulnerable to SPEs, and a partial or total loss of communication satellite function would disrupt telecommunication services, emergency response systems, financial transactions, transportation networks, and weather forecasting abilities among others (65, 66). However, the indirect impacts of an extreme SPE on global climatic and biological systems have generally been overlooked.

While the primary concern regarding extreme SPEs revolves around radiation damage in the upper atmosphere and near-Earth space (3), the direct impact of energetic particles at the surface is minor due to the thickness of the atmosphere (67) and was not considered in this study. The elevated UV-B levels resulting from ozone reduction would be mostly restricted to the polar regions under current geomagnetic conditions, but would still impact global climatic systems. A useful proxy for the potential environmental impacts of a SPE are provided by the chlorofluorocarbon-caused ozone hole detected in the 1980s (68), which altered regional rainfall, cloud cover patterns, and shifted the Southern Annular Mode to a more positive state, with a stronger and more southerly jet stream (69). Further interactions and feedback between ozone decrease, UV radiation, and climate patterns are likely, particularly as future changes in atmospheric circulation and temperature (70) impact the dynamics of the ozone layer, which could worsen the impact of increased UV radiation on ecosystems and human health (52, 71, 72).

The initial biological impacts of increased UV-B levels are expected to be on photosynthesis-utilizing primary producers, such as plants and marine plankton, and accompanying ecosystems. Even small (e.g., 10%) increases in UV radiation can lead to changes in phytoplankton photosynthetic efficiency and growth rates, altering community structure (73). Further interactions between solar radiation, ocean acidification, and generalized warming are likely to substantially influence marine primary producers (74). UV-B is particularly destructive to aquatic microbiomes, including zooplankton and cyanobacteria, as well as eggs and larvae of macroinvertebrates and fish, so even short-term elevated levels are likely to have ecosystem-wide impacts (55, 56).

Since UV-B radiation is the most important risk factor for skin cancer, the modeled increases over continents would likely have significant impacts. The increase in DNA damage rates (>10% over Asia, Europe, and North America, for several years) would not be expected to result in a linear increase in human cancer risk as this depends on individual background and accumulated exposure, including peak and average doses (75). While the amount of sunburn in childhood appears to be a more relevant factor for melanoma than (accumulated) total UV dose (76), the correlation between DNA damage and cancer risk seems more direct for squamous cell carcinoma (77). Nevertheless, DNA damage induction is only the first step in carcinogenesis, and many other factors play decisive roles, e.g., the extent of cell proliferation in the affected tissue (78) type of DNA damage, DNA repair mechanisms, and the cellular DNA damage response, which are modulated by many factors including the accumulated UV dose and dose rate of the UV radiation.

An Extreme SPE during a Geomagnetic Excursion. The extent to which the current geomagnetic field strength provides protection from SPEs is clearly demonstrated by the impacts predicted when geomagnetic field shielding is absent. Widespread ozone depletion and increased UV-B irradiation are expected (Figs. 4–6), with likely serious consequences across global climate and biological systems. Potential climatic effects include significant changes to cloud and snow cover, rainfall patterns, and land and sea temperatures (79), along with feedback from altered phytoplankton growth and food webs in aquatic systems (80, 81). Although the climate model used in this study involves comprehensive atmospheric processes, their investigations involve complex interactions and require extensive analysis, which is beyond the scope of our current study.

A 20 to 25% increase in erythemal radiation would have severe consequences on microbiome and phytoplankton community dynamics and eco-physiological mechanisms, with larger implications for marine food webs and biogeochemical cycling (82). Very high intensities of UV-B radiation could hinder plant growth and photosynthesis and generate elevated levels of DNA damage across many species (83–86). While short-lived, these impacts are likely to cause complex interactions with potentially longer global effects.

Within animals, such high UV levels would be associated with elevated rates of sunburn, cataracts, and DNA damage. These impacts are likely to be particularly severe for humans who lack skin coverings or thick hides, leading to increased risks of skin cancer, cataracts, and impaired immune function as long-term impacts (52). The most immediate negative impact for many animal groups would potentially be damage to the eyes, which would be heightened in environments with reflective surfaces such as snow, savannah, water, or sand (58, 87). In the case of humans, the high UVI (25% increase) exposure could quickly lead to snow blindness, which can manifest anywhere from 30 min to 12 h after the actual exposure (87). The resulting intense pain from exposure to light, severe headaches, and blurry or complete loss of vision would be debilitating to exposed human groups, with the effects lasting for many days and requiring complete avoidance of exposure to light. As such, a SPE during the multiple geomagnetic excursions known in the Late Pleistocene would be expected to have pronounced negative impacts on hunter–forager groups, as has been suggested for the Laschamps and Mono Lake geomagnetic excursions which coincide with major genetic replacement events in European populations (36, 63, 88). For other species, the negative impacts are likely to relate to the extent of preexisting adaptations, such as UV-blocking pigments within eyes. For example, polar or high-altitude species that are exposed to high UV environments would be expected to be better protected or adapted.

Comparing the Effects of SPEs and GSM. In contrast to the short-lived increase in short-wave (high-energy) solar radiation caused by an extreme SPE presented here, the multidecadal impacts of GSM result in less pronounced but much longer-lasting atmospheric drivers (e.g., ref. 89). Well-known historic grand solar minima include the Oort (1040 to 1080), Wolf (1270 to 1350), Spörer (1460 to 1550), Maunder (1645 to 1710), and Dalton (1790 to 1830) Minimum and these have been linked with pronounced Medieval cold periods across European environments (35, 90). Importantly, just as for the case of an extreme SPE, the impacts of a GSM would be much greater during periods of weak geomagnetic field strength. A similar modeling approach (36) has estimated ozone reduction of around 5%, resulting in ground-level UV radiation increases of 10 to 15% during the GSM. While considerably weaker than the effects modeled here, the cumulative impact of 50 to 100 y of GSM atmospheric drivers is expected to result in much larger climatic and biotic responses.

The frequency and duration of geomagnetic excursions apparent in the geological record (along with much less frequent full reversal events) mean that it is likely that many would be coincident with extreme SPE or GSM. Given the severity of the impacts modeled here, the combination of geomagnetic excursions and SPE or GSM are a currently unrecognized and potentially important factor in evolutionary history. In the case of SPE, the short-lived impacts and multiyear consequences are likely to be sufficiently rapid to remain undetectable in most paleorecords prior to the Holocene (<11.6 ka). However, while short-lived, the climatic impacts could have the potential to act as tipping points for ongoing larger-scale climatic processes (e.g., incipient glaciation phases). This combination could produce rapid phase shifts of the sort that are prevalent through Pleistocene paleorecords but remain currently difficult to explain. Similarly for GSM, while the atmospheric effects of at least 9 individual GSM could be discerned in tree ring records of the Laschamps Excursion (36), the overall biological and climatic impacts proposed in that study had not been previously recognized as being linked. These included a marked increase in the use of caves, cave art, and red ochre handprints, suggested to be related to damaging UV-B levels during the Laschamps and consistent with the potential for visual system damage and sunburn outlined here.

The impacts of elevated UV levels on visual systems and DNA damage during repeated or prolonged periods of reduced geomagnetic field strength have also been proposed as a potential factor in major evolutionary transitions. For example, the Late Ediacaran and early Cambrian were characterized by geomagnetic field instability and generally very low field strength, which has been related to the initial formation stages of the Earth's solid iron core (91, 92). The very prolonged periods (e.g., >26 Ma) of low geomagnetic field strength, subsequent atmospheric oxygenation (93), and resulting high levels of UV-B have been proposed as important drivers for the dramatically rapid evolution of complex animal life forms first observed in the early Cambrian period, recorded as the Cambrian Explosion (94, 95). The independent development of visual systems and hard shells across multiple distinct animal phyla contemporaneously has been related to strong selective pressure to detect and avoid damaging levels of UV light. These mechanisms, along with evidence of a marked increase in burrowing behavior under algal mats, have been described as a "flight from light" (94, 95) and are consistent with the impacts modeled here. However, the potential impacts of GSM on evolution remain hypothetical and call for further investigation.

Conclusion

Our interdisciplinary study highlights the importance of understanding the potential impacts of SPEs on the biosphere, both for the current day and through evolutionary history. Given the current limitations in predicting SPEs, there is a need for concerted government and industry action to develop a more comprehensive understanding of these phenomena and their global societal, economic, technological, and ecological implications. This knowledge is important for the development of effective strategies to safeguard infrastructure, maintain essential services, and mitigate the potential risks and consequences of extreme space weather events.

Extreme SPEs are also likely to interact with ongoing climate change, posing additional challenges to ecosystems and human health (52, 71). As Earth's climate continues to change, ecosystems and human societies will become more vulnerable to the impacts of changes in geomagnetic field strength. Future changes in atmospheric circulation and temperature (70) will impact the dynamics of the ozone layer, which could worsen the impact of increased UV radiation. Understanding the impact of extreme SPEs on our atmosphere and developing strategies to address these risks will be important for safeguarding our technological infrastructure and the welfare of the global population.

Materials and Methods

SOCOL3-MPIOM Model Setup. We employ the comprehensive chemistry–climate model SOCOL3-MPIOM (44, 45), which consists of the atmospheric model ECHAM5.4 (96) coupled with the chemistry module MEZON (9, 97) and the ocean model MPIOM (98, 99). Employed as a free-running model, SOCOL was validated against satellite data from the 2003 Halloween SPE (18). SOCOL generally reproduces the observed odd nitrogen NO_y ($N + NO + NO_2 + NO_3 + 2N_2O_5 + HNO_3 + HO_2NO_2 + ClONO_2 + BrONO_2$) levels, with an overestimation of stratospheric NO_y likely due to temperature differences inherent in the model's simulation. SOCOL simulates both mesospheric and stratospheric ozone in a robust fashion, closely matching observations with a minor underestimation of stratospheric ozone loss by around 5%. Our model simulations utilized a grid with a horizontal resolution of 3.75 degrees in latitude and longitude across 39 vertical levels, spanning Earth's surface to the upper mesosphere (approximately 80 km above the surface at the 0.01 hPa pressure level).

We use fixed boundary conditions for greenhouse gases and ozone-depleting substances (CO_2: 185 ppm, CH_4: 200 ppb, N_2O: 350 ppb) (100) based on the Last Glacial Maximum, as an approximation for the climate state during the last major geomagnetic excursion, the Laschamps Event which occurred 42,000 B.P. Tropospheric aerosols are set to low levels to approximate ice-age conditions, while stratospheric aerosols are maintained at background levels. Galactic cosmic rays are parameterized based on geomagnetic latitude, pressure, and solar modulation potential (101). All experiments have identical solar forcing, making the solar modulation potential consistent among them. We conduct four 9-y model experiments, each with 20 ensemble members, varying initial CO_2 concentrations by 0.1% during the first month:

1. The first experiment simulates the geomagnetic conditions of the early 20th-Century (1915 to 1935) (102) with a North geomagnetic pole at 78.5°/291.5° and a geomagnetic field strength (dipole moment) of 8.25×10^{22} Am^2 (103), which is similar value to the stable magnetic field before the Laschamps excursion (27);
2. The second experiment maintains the same boundary conditions as the first but eliminates the geomagnetic field;
3. The third experiment is identical to the first, with the addition of an extreme SPE on day 330 of the first simulation year;
4. The fourth experiment is identical to the second, with the addition of an extreme SPE on day 330 of the first simulation year.

LibRadtran. To calculate the resulting surface UV radiation doses and concomitant health effects, we use the high-resolution model *uvspec* from the LibRadtran package (46), which has been shown to have high accuracy in many intercomparison campaigns (104).

Using LibRadtran, we calculated surface direct spectral solar irradiance from 200 to 800 nm with a resolution of 0.05 nm, applying vertical profiles of temperature, ozone, H_2O, and NO_2 modeled by SOCOL3-MIPOM as the input. The irradiance is then used to calculate changes in surface radiation doses for four action spectra, i.e., for three biological health effects: UV index [International Commission on Illumination-98, CIE-98; (105)], vitamin D production [CIE-174; (64)], and DNA damage (106, 107). We focus on continent-level changes in these parameters as defined in *SI Appendix*, Fig. S1.

SPE. In two of the experiments, we simulated an extreme SPE at the beginning of the boreal (northern) winter (day 330). This specific timing was chosen because the mesospheric SPE-generated NO_x is particularly long-lived in the Northern Hemisphere polar night due to the lack of photolysis, and capable of affecting stratospheric ozone through downwelling air circulation in the polar vortex. This situation permits an analysis of the most extreme SPE impacts on stratospheric ozone, and corresponding alterations in radiation patterns across the Northern Hemisphere. However, if such an event were to occur at the start of the austral winter, the effects on ozone would be more pronounced in the Southern Hemisphere.

Ionization rates from the SPE in the atmosphere were determined using the cosmic-ray-induced ionization model CRAC:CRII (101, 108). The production of NO_x by SPEs yields 0.55 molecules of ground state N per ion pair, while a greater proportion,

0.7 molecules per ion pair, results in the excited N state, which almost immediately reacts with O_2 to produce NO (109, 110). Additionally, we account for the formation of up to two HO_x molecules per ionization rate, with variations by altitude (111).

We select a conservative upper limit of SPE total particle energy (112) for a worst-case scenario, corresponding to the SPE in the year 775, which is one of the most intense SPEs in the Holocene (<11.8 ka). This event's intensity is estimated to be 70 ± 30 times greater (5) than the most powerful SPE recorded in recent history, which took place on February 23, 1956 (113).

Geomagnetic Field. Although the global geomagnetic field parameters are relatively well known for the Laschamps excursion (27, 114), the magnetospheric state remains uncertain due to an absence of precise magnetohydrodynamical modeling. In particular, it is unclear whether precipitating particles from radiation belts and auroral electrons existed during this period in Earth's history.

In our study, following earlier methodology (36, 39), we assume the total disappearance of the geomagnetic field during the excursion, given that the actual field configuration is unknown. Although some studies estimate that the dipole field strength during a geomagnetic reversal/excursion can reduce to a few percent of current values (27, 115), the nondipole component can remain significant. This nonuniformity could increase ionization in specific areas by directing or focusing energetic particles at certain points, but a lack of appropriate models meant that this contribution could not be included in this study.

Overall, the conditions modeled here provide boundaries for estimating the impacts of an extreme SPE under different geomagnetic field strengths, ranging from the current strong conditions to total field collapse.

Data, Materials, and Software Availability. Model outputs data have been deposited in Mendeley Data (10.17632/szmx77j4vz.1) (116).

ACKNOWLEDGMENTS. We extend our gratitude to Prof. Dr. Bernd Epe from Johannes Gutenberg Universität Mainz for assistance regarding the UV effect and Dr. Urs Beyerle from ETH Zürich for the IT support. T.E. and T.S. acknowledge support from the Swiss National Science Foundation (SNSF) project AEON (grant no. 200020E_219166) and Karbacher Fonds, Graubünden, Switzerland. T.E. also has been supported by the SNSF SPARC project GECO (grant no. CRSK-2_221368). E.R. acknowledges a support from SPBU (grant ID 116234986). I.U. acknowledges partial support from the Academy of Finland (project No. 354280) and fruitful discussions within the ISSI International Team #510 (SEESUP Solar Extreme Events: Setting Up a Paradigm). C.T. and A.C. acknowledge support from the Australian Research Council (ARC DP170104665 and Laureate Fellowships). Simulations have been performed on the ETH Zürich cluster Euler.

Author affiliations: [a]Institute of Meteorology and Climatology, Department of Water, Atmosphere, and Environment, BOKU University, Vienna 1180, Austria; [b]Institute for Atmospheric and Climate Science, ETH, Zürich 8092, Switzerland; [c]Physikalisch-Meteorologisches Observatorium Davos und World Radiation Center (PMOD/WRC), Davos 7260, Switzerland; [d]Ozone Layer and Upper Atmosphere Research Laboratory, Saint-Petersburg State University, Saint-Petersburg 198504, Russia; [e]Space Physics and Astronomy Research Unit, University of Oulu, Oulu 90014, Finland; [f]Institute for Sustainable Futures, Division of Research, University of Technology Sydney, Ultimo, NSW 2007, Australia; [g]Federal Office of Meteorology and Climatology, MeteoSwiss, Zurich 8058, Switzerland; [h]Water, Energy and Environmental Engineering Research Unit, University of Oulu, Oulu 90014, Finland; [i]Geophysics Department, Helmholtz-Zentrum Potsdam – Deutsches GeoForschungsZentrum GFZ German Research Centre for Geosciences, Potsdam 14473, Germany; and [j]Gulbali Institute, Charles Sturt University, Albury, NSW 2640, Australia

Author contributions: P.A., E.R., and T.S. designed research; P.A. performed research; P.A., E.R., I.U., C.T., T.S., K.M., M.F., J.A., S.S., V.M., T.E., M.K., H.R., A.C., and T.P. participated in the data analysis and interpretation; and P.A. and A.C. wrote the paper with input from all co-authors.

1. M. Desai, J. Giacalone, Large gradual solar energetic particle events. *Living Rev. Sol. Phys.* **13**, 3 (2016).
2. I. A. Mironova *et al.*, Energetic particle influence on the Earth's atmosphere. *Space Sci. Rev.* **194**, 1–96 (2015).
3. F. Miyake, I. Usoskin, S. Poluianov, Eds., *Extreme Solar Particle Storms: The Hostile Sun* (IOP Publishing, 2019).
4. R. Vainio *et al.*, Dynamics of the Earth's particle radiation environment. *Space Sci. Rev.* **147**, 187–231 (2009).
5. E. W. Cliver, C. J. Schrijver, K. Shibata, I. G. Usoskin, Extreme solar events. *Living Rev. Sol. Phys.* **19**, 2 (2022).
6. N. Brehm *et al.*, Tree-rings reveal two strong solar proton events in 7176 and 5259 BCE. *Nat. Commun.* **13**, 1196 (2022).
7. I. G. Usoskin, G. A. Kovaltsov, Occurence of extreme solar particle events: Assessment from historical proxy data. *ApJ* **757**, 92 (2012).
8. B. T. Tsurutani, The extreme magnetic storm of 1–2 September 1859. *J. Geophys. Res.* **108**, 1268 (2003).
9. T. Egorova, E. Rozanov, V. Zubov, I. Karol, Model for investigating ozone trends (MEZON). *Izv. Atmos. Oceanic Phys.* **39**, 277–292 (2003).
10. P. J. Crutzen, I. S. A. Isaksen, G. C. Reid, Solar proton events: Stratospheric sources of nitric oxide. *Science* **189**, 457–459 (1975).
11. H. S. Porter, C. H. Jackman, A. E. S. Green, Efficiencies for production of atomic nitrogen and oxygen by relativistic proton impact in air. *J. Chem. Phys.* **65**, 154–167 (1976).
12. S. Solomon, D. W. Rusch, J. C. Gérard, G. C. Reid, P. J. Crutzen, The effect of particle precipitation events on the neutral and ion chemistry of the middle atmosphere: II. Odd hydrogen. *Planet. Space Sci.* **29**, 885–893 (1981).
13. W. Swider, T. J. Keneshea, Decrease of ozone and atomic oxygen in the lower mesosphere during a PCA event. *Planet. Space Sci.* **21**, 1969–1973 (1973).
14. B. Funke *et al.*, Enhancement of N2O during the October–November 2003 solar proton events. *Atmos. Chem. Phys.* **8**, 3805–3815 (2008), https://doi.org/10.5194/acp-8-3805-2008.
15. C. E. Randall, D. E. Siskind, R. M. Bevilacqua, Stratospheric NO_x enhancements in the Southern Hemisphere Vortex in winter/spring of 2000. *Geophys. Res. Lett.* **28**, 2385–2388 (2001).
16. A. Seppälä, M. A. Clilverd, C. J. Rodger, NO_x enhancements in the middle atmosphere during 2003–2004 polar winter: Relative significance of solar proton events and the aurora as a source. *J. Geophys. Res.* **112**, D23303 (2007).
17. R. D. McPeters, C. H. Jackman, E. G. Stassinopoulos, Observations of ozone depletion associated with solar proton events. *J. Geophys. Res.* **86**, 12071 (1981).
18. B. Funke *et al.*, Composition changes after the "Halloween" solar proton event: The High Energy Particle Precipitation in the Atmosphere (HEPPA) model versus MIPAS data intercomparison study. *Atmos. Chem. Phys.* **11**, 9089–9139 (2011).
19. C. H. Jackman *et al.*, Northern Hemisphere atmospheric influence of the solar proton events and ground level enhancement in January 2005. *Atmos. Chem. Phys.* **11**, 6153–6166 (2011).
20. T. Sukhodolov *et al.*, Atmospheric impacts of the strongest known solar particle storm of 775 AD. *Sci. Rep.* **7**, 45257 (2017).
21. N. Kalakoski, P. T. Verronen, M. E. Szeląg, C. H. Jackman, Global ozone loss following extreme solar proton storms based on the July 2012 coronal mass ejection. *Sci. Rep.* **13**, 13873 (2023).
22. M. Landeau, A. Fournier, H.-C. Nataf, D. Cébron, N. Schaeffer, Sustaining Earth's magnetic dynamo. *Nat. Rev. Earth Environ.* **3**, 255–269 (2022).
23. J. S. Gee, D. V. Kent, "Source of oceanic magnetic anomalies and the geomagnetic polarity timescale" in *Treatise on Geophysics*, G. Schubert, Ed. (Elsevier, 2007), pp. 419–460.
24. D. Gubbins, Mechanism for geomagnetic polarity reversals. *Nature* **326**, 167–169 (1987).
25. G. Hulot, C. Eymin, B. Langlais, M. Mandea, N. Olsen, Small-scale structure of the geodynamo inferred from Oersted and Magsat satellite data. *Nature* **416**, 620–623 (2002).
26. C. Laj, J. E. T. Channell, "Geomagnetic excursions" in *Treatise on Geophysics*, G. Schubert, Ed. (Elsevier, 2015), pp. 343–383.
27. M. Korte, M. C. Brown, S. Panovska, I. Wardinski, Robust characteristics of the Laschamp and Mono Lake geomagnetic excursions: Results from global field models. *Front. Earth Sci.* **7**, 86 (2019).
28. N. Olsen *et al.*, The Swarm initial field model for the 2014 geomagnetic field. *Geophys. Res. Lett.* **42**, 1092–1098 (2015).
29. C. Laj, C. Kissel, An impending geomagnetic transition? Hints from the past *Front. Earth Sci.* **3**, 61 (2015).
30. F. J. Pavón-Carrasco, A. De Santis, The South Atlantic Anomaly: The key for a possible geomagnetic reversal. *Front. Earth Sci.* **4**, 40 (2016).
31. A. P. Roberts, Geomagnetic excursions: Knowns and unknowns. *Geophys. Res. Lett.* **35**, L17307 (2008).
32. B. S. Singer, A Quaternary geomagnetic instability time scale. *Q. Geochronol.* **21**, 29–52 (2014).
33. S. Panovska, C. G. Constable, M. Korte, Extending global continuous geomagnetic field reconstructions on timescales beyond human civilization. *Geochem. Geophys. Geosyst.* **19**, 4757–4772 (2018).
34. I. G. Usoskin, S. K. Solanki, G. A. Kovaltsov, Grand minima and maxima of solar activity: New observational constraints. *Astron. Astrophys.* **471**, 301–309 (2007).
35. F. Sirocko, H. Brunck, S. Pfahl, Solar influence on winter severity in central Europe. *Geophys. Res. Lett.* **39**, 2012GL052412 (2012).
36. A. Cooper *et al.*, A global environmental crisis 42,000 years ago. *Science* **371**, 811–818 (2021).
37. D. Hauglustaine, J.-C. Gerard, Possible composition and climatic changes due to past intense energetic particle precipitation. *Ann. Geophys.* **8**, 87–96 (1990).
38. G. C. Reid, I. S. A. Isaksen, T. E. Holzer, P. J. Crutzen, Influence of ancient solar-proton events on the evolution of life. *Nature* **259**, 177–179 (1976).
39. M. Sinnhuber *et al.*, A model study of the impact of magnetic field structure on atmospheric composition during solar proton events. *Geophys. Res. Lett.* **30**, 1818 (2003).
40. M. Calisto, I. Usoskin, E. Rozanov, Influence of a Carrington-like event on the atmospheric chemistry, temperature and dynamics: Revised. *Environ. Res. Lett.* **8**, 045010 (2013).
41. T. Reddmann, M. Sinnhuber, J. M. Wissing, O. Yakovchuk, I. Usoskin, The impact of an extreme solar event on the middle atmosphere: A case study. *Atmos. Chem. Phys.* **23**, 6989–7000 (2023).
42. S. Koldobskiy, F. Mekhaldi, G. Kovaltsov, I. Usoskin, Multiproxy reconstructions of integral energy spectra for extreme solar particle events of 7176 BCE, 660 BCE, 775 CE, and 994 CE. *JGR Space Phys.* **128**, e2022JA031186 (2023).
43. K.-H. Glassmeier, J. Vogt, Magnetic polarity transitions and biospheric effects: Historical perspective and current developments. *Space Sci. Rev.* **155**, 387–410 (2010).
44. S. Muthers *et al.*, The coupled atmosphere-chemistry-ocean model SOCOL-MPIOM. *Geosci. Model Dev. Discuss.* **7**, 3013–3084 (2014).
45. A. Stenke *et al.*, The SOCOL version 3.0 chemistry–climate model: Description, evaluation, and implications from an advanced transport algorithm. *Geosci. Model Dev.* **6**, 1407–1427 (2013).
46. C. Emde *et al.*, The libRadtran software package for radiative transfer calculations (version 2.0.1). *Geosci. Model Dev.* **9**, 1647–1672 (2016).

47. T. Egorova *et al.*, The atmospheric effects of October 2003 solar proton event simulated with the chemistry–climate model SOCOL using complete and parameterized ion chemistry. *J. Atmos. Sol.-Terr. Phys.* **73**, 356–365 (2011).
48. E. Mayor, A. M. Velasco, I. Martín, Photodissociation of the δ (0,0) and δ (1,0) bands of nitric oxide in the stratosphere and the mesosphere: A molecular-adapted quantum defect orbital calculation of photolysis rate constants. *J. Geophys. Res.* **112**, 2007JD008643 (2007).
49. G. Brasseur, S. Solomon, *Aeronomy of the Middle Atmosphere: Chemistry and Physics of the Stratosphere and Mesosphere* (Springer, Third revised and enlarged edition, 2005).
50. C. H. Jackman, E. L. Fleming, F. M. Vitt, Influence of extremely large solar proton events in a changing stratosphere. *J. Geophys. Res.* **105**, 11659–11670 (2000).
51. R. J. Van Der A, M. A. F. Allaart, H. J. Eskes, Extended and refined multi sensor reanalysis of total ozone for the period 1970–2012. *Atmos. Meas. Tech.* **8**, 3021–3035 (2015).
52. R. E. Neale *et al.*, Environmental effects of stratospheric ozone depletion, UV radiation, and interactions with climate change: UNEP Environmental Effects Assessment Panel, Update 2020. *Photochem. Photobiol. Sci.* **20**, 1–67 (2021).
53. H. Ikehata *et al.*, Action spectrum analysis of UVR genotoxicity for skin: The border wavelengths between UVA and UVB can bring serious mutation loads to skin. *J. Investigat. Dermatol.* **133**, 1850–1856 (2013).
54. H. Ikehata *et al.*, Wavelength- and tissue-dependent variations in the mutagenicity of cyclobutane pyrimidine dimers in mouse skin. *Photochem. Photobiol.* **96**, 94–104 (2020).
55. C. E. Williamson *et al.*, The interactive effects of stratospheric ozone depletion, UV radiation, and climate change on aquatic ecosystems. *Photochem. Photobiol. Sci.* **18**, 717–746 (2019).
56. D.-P. Häder, E. W. Helbling, C. E. Williamson, R. C. Worrest, Effects of UV radiation on aquatic ecosystems and interactions with climate change. *Photochem. Photobiol. Sci.* **10**, 242–260 (2011).
57. J. F. Sánchez-Pérez, D. Vicente-Agullo, M. Barberá, E. Castro-Rodríguez, M. Cánovas, Relationship between ultraviolet index (UVI) and first-, second- and third-degree sunburn using the Probit methodology. *Sci. Rep.* **9**, 733 (2019).
58. N. Hatsusaka *et al.*, UV index does not predict ocular ultraviolet exposure. *Trans. Vis. Sci. Tech.* **10**, 1 (2021).
59. R. Chadyšienė, A. Girgždys, Ultraviolet radiation albedo of natural surfaces. *J. Environ. Eng. Landscape Manage.* **16**, 83–88 (2008).
60. P. H. Hart, S. Gorman, J. J. Finlay-Jones, Modulation of the immune system by UV radiation: More than just the effects of vitamin D? *Nat. Rev. Immunol.* **11**, 584–596 (2011).
61. R. Vieth, Vitamin D supplementation, 25-hydroxyvitamin D concentrations, and safety. *Am. J. Clin. Nutr.* **69**, 842–856 (1999).
62. J. Rocha, The evolutionary history of human skin pigmentation. *J Mol. Evol.* **88**, 77–87 (2020).
63. R. Tobler *et al.*, The role of genetic selection and climatic factors in the dispersal of anatomically modern humans out of Africa. *Proc. Natl. Acad. Sci. U.S.A.* **120**, e2213061120 (2023).
64. I. Terenetskaya, "Inter-relation between the in vivo and in vitro action spectra of vitamin D synthesis" in *Proceedings of the 2nd Cie Expert Symposium on Lighting and Health* (Ottawa, Canada, 2006), pp. 182–185.
65. J. P. Eastwood *et al.*, The economic impact of space weather: Where do we stand?: Perspective. *Risk Anal.* **37**, 206–218 (2017).
66. C. J. Schrijver *et al.*, Understanding space weather to shield society: A global road map for 2015–2025 commissioned by COSPAR and ILWS. *Adv. Space Res.* **55**, 2745–2807 (2015).
67. A. Mishev, S. Panovska, I. Usoskin, Assessment of the radiation risk at flight altitudes for an extreme solar particle storm of 774 AD. *J. Space Weather Space Clim.* **13**, 22 (2023).
68. J. C. Farman, B. G. Gardiner, J. D. Shanklin, Large losses of total ozone in Antarctica reveal seasonal ClOx/NOx interaction. *Nature* **315**, 207–210 (1985).
69. P. W. Barnes *et al.*, Environmental effects of stratospheric ozone depletion, UV radiation, and interactions with climate change: UNEP Environmental Effects Assessment Panel, Update 2021. *Photochem. Photobiol. Sci.* **21**, 275–301 (2022).
70. P. Arsenovic *et al.*, Implications of potential future grand solar minimum for ozone layer and climate. *Atmos. Chem. Phys.* **18**, 3469–3483 (2018).
71. R. L. McKenzie *et al.*, Ozone depletion and climate change: Impacts on UV radiation. *Photochem. Photobiol. Sci.* **10**, 182–198 (2011).
72. J. F. Bornman *et al.*, Linkages between stratospheric ozone, UV radiation and climate change and their implications for terrestrial ecosystems. *Photochem. Photobiol. Sci.* **18**, 681–716 (2019).
73. D.-P. Häder *et al.*, Effects of UV radiation on aquatic ecosystems and interactions with other environmental factors. *Photochem. Photobiol. Sci.* **14**, 108–126 (2014).
74. K. Gao, E. Helbling, D. Häder, D. Hutchins, Responses of marine primary producers to interactions between ocean acidification, solar radiation, and warming. *Mar. Ecol. Prog. Ser.* **470**, 167–189 (2012).
75. R. Gordon, Skin cancer: An overview of epidemiology and risk factors. *Semin. Oncol. Nurs.***29**, 160–169 (2013).
76. D. Whiteman, A. Green, Melanoma and sunburn. *Cancer Causes Control* **5**, 564–572 (1994).
77. P. M. Rodust, E. Stockfleth, C. Ulrich, M. Leverkus, J. Eberle, UV-induced squamous cell carcinoma–A role for antiapoptotic signalling pathways. *Br. J. Dermatol.* **161**, 107–115 (2009).
78. M. R. Hussein, Ultraviolet radiation and skin cancer: Molecular mechanisms. *J. Cutan. Pathol.* **32**, 191–205 (2005).
79. R. G. Harrison, M. Lockwood, Rapid indirect solar responses observed in the lower atmosphere. *Proc. R. Soc. A* **476**, 20200164 (2020).
80. C. Martin-Puertas *et al.*, Regional atmospheric circulation shifts induced by a grand solar minimum. *Nat. Geosci.* **5**, 397–401 (2012).
81. R. Thiéblemont, K. Matthes, N.-E. Omrani, K. Kodera, F. Hansen, Solar forcing synchronizes decadal North Atlantic climate variability. *Nat. Commun.* **6**, 8268 (2015).
82. P. Carrillo *et al.*, Interactive effect of UVR and phosphorus on the coastal phytoplankton community of the Western Mediterranean Sea: Unravelling eco-physiological mechanisms. *PLoS One* **10**, e0142987 (2015).
83. P. Balint-Kurti, S. J. Simmons, J. E. Blum, C. L. Ballaré, A. E. Stapleton, Maize leaf epiphytic bacteria diversity patterns are genetically correlated with resistance to fungal pathogen infection. *Mol. Plant Microbe Interact.* **23**, 473–484 (2010).
84. G. Berg, T. Cernava, The plant microbiota signature of the Anthropocene as a challenge for microbiome research. *Microbiome* **10**, 54 (2022).
85. L. Janette, G. W. Sundin, Effect of solar UV-B radiation on a phyllosphere bacterial community. *Appl. Environ. Microbiol.* **67**, 5488–5496 (2001).
86. A. Yadav *et al.*, Light signaling and UV-B-mediated plant growth regulation. *J. Integr. Plant Biol.* **62**, 1270–1292 (2020).
87. L. A. Moore, M. Hussey, J. T. Ferreira, B. Wu, Review of photokeratitis: Corneal response to ultraviolet radiation (UVR) exposure. *Afr. Vision Eye Health* **69**, 123–131 (2010).
88. A. Cooper *et al.*, Response to Comment on "A global environmental crisis 42,000 years ago". *Science* **374**, eabi9756 (2021).
89. J. G. Anet *et al.*, Impact of solar versus volcanic activity variations on tropospheric temperatures and precipitation during the Dalton Minimum. *Clim. Past* **10**, 921–938 (2014).
90. M. E. Mann *et al.*, Global signatures and dynamical origins of the little ice age and medieval climate anomaly. *Science* **326**, 1256–1260 (2009).
91. R. K. Bono, J. A. Tarduno, F. Nimmo, R. D. Cottrell, Young inner core inferred from Ediacaran ultra-low geomagnetic field intensity. *Nat. Geosci.* **12**, 143–147 (2019).
92. S. J. Lloyd, A. J. Biggin, G. A. Paterson, P. J. A. McCausland, Extremely weak early Cambrian dipole moment similar to Ediacaran: Evidence for long-term trends in geomagnetic field behaviour? *Earth Planet. Sci. Lett.* **595**, 117757 (2022).
93. W. Huang *et al.*, Near-collapse of the geomagnetic field may have contributed to atmospheric oxygenation and animal radiation in the Ediacaran Period. *Commun. Earth Environ.* **5**, 207 (2024).
94. J. G. Meert, N. M. Levashova, M. L. Bazhenov, E. Landing, Rapid changes of magnetic Field polarity in the late Ediacaran: Linking the Cambrian evolutionary radiation and increased UV-B radiation. *Gondwana Res.* **34**, 149–157 (2016).
95. C. Doglioni, J. Pignatti, M. Coleman, Why did life develop on the surface of the Earth in the Cambrian? *Geosci. Front.* **7**, 865–873 (2016).
96. E. Roeckner *et al.*, The atmospheric general circulation model ECHAM5: Part 1: Model description. *MPI Rep.* **349**, 1–140 (2003).
97. E. V. Rozanov, V. A. Zubov, M. E. Schlesinger, F. Yang, N. G. Andronova, The UIUC three-dimensional stratospheric chemical transport model: Description and evaluation of the simulated source gases and ozone. *J. Geophys. Res.* **104**, 11755 (1999).
98. J. H. Jungclaus *et al.*, Ocean circulation and tropical variability in the coupled model ECHAM5/MPI-OM. *J. Clim.* **19**, 3952–3972 (2006).
99. S. J. Marsland, H. Haak, J. H. Jungclaus, M. Latif, F. Röske, The Max-Planck-Institute global ocean/sea ice model with orthogonal curvilinear coordinates. *Ocean Model.* **5**, 91–127 (2002).
100. M. Klockmann, *The AMOC and Its Sensitivity to Different Climate Forcings in the Range of Glacial to Modern Conditions* (Max-Planck-Institut für Meteorologie, Hamburg, 2017).
101. I. G. Usoskin, G. A. Kovaltsov, I. A. Mironova, Cosmic ray induced ionization model CRAC:CRII: An extension to the upper atmosphere. *J. Geophys. Res.* **115**, D10302 (2010).
102. P. Alken *et al.*, International geomagnetic reference field: The thirteenth generation. *Earth Planets Space* **73**, 49 (2021).
103. A. A. Schreider, A. A. Schreider, P. Varga, C. Denis, Evolution of the virtual dipole moment through the Paleoarchean–Phanerozoic. *Oceanology* **55**, 245–252 (2015).
104. B. Mayer, A. Kylling, Technical note: The libRadtran software package for radiative transfer calculations–Description and examples of use. *Atmos. Chem. Phys.* **5**, 1855–1877 (2005), https://doi.org/10.5194/acp-5-1855-2005.
105. A. R. Webb, H. Slaper, P. Koepke, A. W. Schmalwieser, Know your standard: Clarifying the CIE erythema action spectrum. *Photochem. Photobiol.* **87**, 483–486 (2011).
106. R. B. Setlow, The wavelengths in sunlight effective in producing skin cancer: A theoretical analysis. *Proc. Natl. Acad. Sci. U.S.A.* **71**, 3363–3366 (1974).
107. G. Bernhard, B. Mayer, G. Seckmeyer, A. Moise, Measurements of spectral solar UV irradiance in tropical-Australia. *J. Geophys. Res.* **102**, 8719–8730 (1997).
108. I. G. Usoskin, G. A. Kovaltsov, Cosmic ray induced ionization in the atmosphere: Full modeling and practical applications. *J. Geophys. Res.* **111**, 2006JD007150 (2006).
109. C. H. Jackman *et al.*, Neutral atmospheric influences of the solar proton events in October–November 2003. *J. Geophys. Res.* **110**, 2004JA010888 (2005).
110. C. H. Jackman *et al.*, Short- and medium-term atmospheric constituent effects of very large solar proton events. *Atmos. Chem. Phys.* **8**, 765–785 (2008).
111. S. Solomon, D. W. Rusch, J. C. Gérard, G. C. Reid, P. J. Crutzen, The effect of particle precipitation events on the neutral and ion chemistry of the middle atmosphere: II. Odd hydrogen. *Planet. Space Sci.* **29**, 885–893 (1981).
112. K. Golubenko, E. Rozanov, I. Mironova, A. Karagodin, I. Usoskin, Natural sources of ionization and their impact on atmospheric electricity. *Geophys. Res. Lett.* **47**, e2020GL088619 (2020).
113. I. G. Usoskin *et al.*, Revisited reference solar proton event of 23 February 1956: Assessment of the cosmogenic-isotope method sensitivity to extreme solar events. *JGR Space Phys.* **125**, e2020JA027921 (2020).
114. J. Gao, M. Korte, S. Panovska, Z. Rong, Y. Wei, Effects of the laschamps excursion on geomagnetic cutoff rigidities. *Geochem. Geophys. Geosyst.* **23**, e2021GC010261 (2022).
115. J. Vogt *et al.*, Energetic particles in the paleomagnetosphere: Reduced dipole configurations and quadrupolar contributions. *J. Geophys. Res.* **112**, 2006JA012224 (2007).
116. P. Arsenović, Data from "Global impacts of an extreme solar particle event under different geomagnetic field strengths." Mendeley Data, V1. https://data.mendeley.com/datasets/szmx77j4vz/1. Accessed 6 June 2024.